Carbohydrate Polymers 101 (2014) 68–74

Contents lists available at ScienceDirect

Carbohydrate Polymers

journal homepage: www.elsevier.com/locate/carbpol

Electrospinning and characterization of chitin nanofibril/polycaprolactone nanocomposite fiber mats

Yali Ji[a,*], Kai Liang[b], Xinyuan Shen[a], Gary L. Bowlin[c,**]

[a] State Key Laboratory for Modification of Chemical Fibers and Polymer Materials, College of Material Science and Engineering, Donghua University, Shanghai 201620, China
[b] College of Chemistry, Chemical Engineering and Biotechnology, Donghua University, Shanghai 201620, China
[c] Department of Biomedical Engineering, Virginia Commonwealth University, Richmond, VA 23284, USA

ARTICLE INFO

Article history:
Received 29 May 2012
Received in revised form 28 August 2012
Accepted 4 September 2013
Available online 14 September 2013

Keywords:
Chitin nanofibril
Polycaprolactone
Electrospinning
Nanocomposite

ABSTRACT

Nanocomposite fiber mats based on biodegradable polycaprolactone (PCL) and chitin nanofibril (n-chitin) were produced via electrospinning. The morphologies, thermal and mechanical properties as well as surface wettability of the fiber mats were studied by scanning electron microscopy, differential scanning calorimetry analysis, thermogravimetric analysis, dynamic mechanical analysis and static water-contact-angle analysis, respectively. The addition of chitin nanofibrils into PCL resulted in a small change in thermal behavior, but a significant improvement in mechanical properties. Moreover, the surface wettability of electrospun fiber mats transformed from hydrophobicity to hydrophilicity when the chitin nanofibril content was more than 25 wt%. In addition, in vitro cell culture results indicated that the addition of chitin nanofibrils can strongly improve the cellular infiltration and migration confirming that the chitin nanofibril was a good reinforcing as well as bioactive filler for PCL.

1. Introduction

Poly(ε-caprolactone) (PCL) is a commonly used biodegradable, low-priced biopolymer applied to a variety of FDA-approved products. It is tough, flexible and biocompatible, and recently it has attracted much interest because of its potential applications in the field of tissue engineering (Cipitria, Skelton, Dargaville, Daltona, & Hutmacher, 2011; McClure, Sell, Simpson, Walpoth, & Bowlin, 2010; Woodruff & Hutmacher, 2010). PCL possesses superior rheological and viscoelastic properties and can be easily manufactured and manipulated into a large range of scaffolds. Electrospinning is a rather simple and promising technique to fabricate scaffolds, since the resulting microstructures of fiber mats are similar to the extracellular matrix (ECM) so as to facilitate the design of surgical implants that promote tissue regeneration. PCL has been shown to be particularly useful for the production of electrospun fibers to mimic ECM (Cipitria et al., 2011). However, a few challenges are encountered by using PCL as a scaffold material, such as its hydrophobic nature, lack of bioactivity and limited mechanical strength, thus many efforts have been made to improve its properties. For example, blending PCL with hydrophilic biopolymers is usually aimed at facilitating cell adhesion (Lee et al., 2008); preparing PCL-based nanocomposites by loading inorganic reinforcing nano-fillers such as bioglass (Jo et al., 2009), calcium phosphate (Chen & Chang, 2011; Erisken, Kalyon, & Wang, 2008), forsterite (Diba, Fathi, & Kharaziha, 2011) and carbon nanotube (Saeed, Park, Lee, Baek, & Huh, 2006), is commonly trying to improve the mechanical properties of PCL-based scaffolds. The biological materials, such as surface-modified cellulose nanocrystals (Zoppe, Peresin, Habibi, Venditti, & Rojas, 2009) have also been reported as a reinforcing agent for PCL. Chitin is the second most abundant biopolymer next to cellulose and possesses many favorable properties such as non-toxicity, high crystallinity, biocompatibility and biodegradability (Dufresne, 2008). Acid-treatment of chitin can dissolve away regions of low lateral order, resulting in elongated rod-like nanoparticles, termed "nanofibrils" (otherwise called whiskers, or nanocrystals). Besides traditional acid-treatment, there are several other approaches to obtain chitin nanofibrils (n-chitin) (Fan, Saito, & Isogai, 2008; Ifuku et al., 2009; Kadokawa, Takegawa, Mine, & Prasad, 2011). Muzzarelli (2011a, 2011b, 2011c, 2011d) reviewed the recent advances in chitin nanofibril and its preparation technique in detail. Chitin nanofibril is an emerging, novel nanofiller, and has been shown to bring about reinforcing effects on both synthetic and natural polymeric structures (Junkasem, Rujiravanit, Grady, & Supaphol, 2010; Lu, Weng, & Zhang, 2004; Paillet & Dufresne, 2001; Sriupayo, Supaphol, Blackwell, & Rujiravanit, 2005; Wongpanit et al., 2007). The good biocompatibility and biodegradability also make it one of the most promising fillers. However,

* Corresponding author. Tel.: +86 21 6779 2941; fax: +86 21 6779 2855.
** Corresponding author. Tel.: +1 804 828 2592; fax: +1 804 828 4454.
E-mail addresses: jiyali@dhu.edu.cn (Y. Ji), glbowlin@vcu.edu (G.L. Bowlin).

0144-8617/$ – see front matter © 2013 Elsevier Ltd. All rights reserved.
http://dx.doi.org/10.1016/j.carbpol.2013.09.012

it was thought that chitin nanofibrils could only disperse well in aqueous solution, and disperse poorly in organic solvents, which to some extent restricted the development of chitin nanofibril-based nanocomposites. In a previous study (Ji, Wolfe, Rodriguez, & Bowlin, 2012), we found that the chitin nanofibril could disperse in 2,2,2-trifluoroethanol (TFE) solvent and TFE was also a good solvent for PCL, thus we prepared n-chitin/PCL nanocomposites (cast films and fiber mats) and confirmed the practicability of using TFE as cosolvent to prepare n-chitin based nanocomposites. In this work, we further investigated the morphologies, the thermal and mechanical properties, the surface wettability as well as biological property of the electrospun n-chitin/PCL nanocomposite fiber mat systematically, expecting it to be a potential candidate for a tissue engineering scaffold.

2. Experimental

2.1. Preparation of chitin nanofibril

Chitin nanofibril suspension were prepared according to Dufresne's method (Dufresne, 2008) with minor modification. Briefly, chitin flakes were hydrolyzed in 3 N HCl under stirring and refluxing for 6 h. The ratio of the 3 N HCl solution to chitin was 30 $cm^3\ g^{-1}$. The residue was collected after centrifugation and treated twice with 3 N HCl. Then, the residue was washed with deionized water three times by centrifuging and decanting the supernatant. The obtained suspension was further dialyzed in deionized water at room temperature for 3 days, followed by ultrasonic treatment (Whaledent Biosonic Ultrasonicator, USA) for 20 min and subsequent filtration to remove residual aggregates. Finally, the clear suspension was lyophilized to obtain light yellow powders. The yield was 55%. The reason why we utilized chitin nanofibril powders not chitin nanofibril aqueous suspension was that the powders were easier to accurately weigh and redisperse in solvents.

2.2. Electrospinning of n-chitin/PCL nanocomposite fiber mats

A desired amount of chitin nanofibril powders were redispersed in deionized water by sonicating for 30 min, followed by solvent-exchanging from water to acetone followed by centrifugation. The paste of chitin nanofibrils was then well dispersed in TFE (TCI America Inc., USA) by sonicating for 30 min, finally, a colloidal suspension was obtained; PCL (M_n = 80 000 g mol^{-1}; Fluka, USA) was dissolved in TFE under shaking overnight. The two parts were mixed together and further sonicated for 30 min. A clear mixture was then obtained. The mass ratios of chitin nanofibril filler to PCL were controlled at 0:100, 5:95, 10:90, 15:85, 20:80, 25:75 and 30:70. The total concentration of chitin nanofibril and PCL was kept 10 wt%, and PCL concentration varied according to chitin nanofibril. The mixture was loaded into a 5 cm^3 plastic syringe fitted with 18-gauge blunt-tipped needle, and dispensed at 1 $cm^3\ h^{-1}$ using a syringe pump. The applied potential was fixed at 20 kV, the distance between the needle tip and the grounded mandrel (cylindrical, diameter = 2.5 cm) was 15 cm, and mandrel rotation speed was 400 rpm.

2.3. Measurement and characterization

Transmission electron microscopy (TEM) was used to evaluate the morphology and dispersibility of chitin nanofibrils. A drop of diluted chitin nanofibril suspension in TFE was cast onto a carbon coated copper grid, slowly evaporated at room temperature, and then observed on a JEOL JEM-1230 transmission electron microscope.

The morphologies of electrospun fiber mats were observed on a JEOL JSM-5610LV scanning electron microscope (SEM). The fiber diameters and distributions were determined by the ImageJ 1.42 software. Means and standard deviations were determined from 80 measurements of fiber diameter.

Fourier transform infrared spectroscopy (FTIR) spectra were measured (reflection) on a Nicolet 670 Nexus FTIR Spectrometer at 4 cm^{-1} resolution.

Wide angle X-ray diffraction (WAXD) patterns were recorded on a PANalytical X'pert PRO diffractometer at room temperature operated at 45 kV and 40 mA. The scan speed was 3° min^{-1} in the range of 5–45°.

Differential scanning calorimetry (DSC) measurements were performed on a DSC Q20 (TA Instruments, New Castle, DE, USA). Samples were heated from −80 to 100 °C at a heating rate of 10 °C min^{-1} under a nitrogen atmosphere. Each test was repeated three times and obtained data were averaged.

Thermogravimetric analysis (TGA) was carried on a STA 409PC simultaneous thermal analysis system (Netzsch STA Instruments, Germany) to investigate the thermal stability of the nanocomposites. The scanning range was 25–550 °C with a heating rate of 10 °C min^{-1} under a nitrogen atmosphere.

Dynamics mechanical analysis (DMA) were carried out on a TA Rheometrics Solids Analyzer (RSA-III) performing at 1 Hz frequency and a heating rate of 5 °C min^{-1} from −90 to 200 °C in a tension mode. The specimens with thickness about 0.2–0.3 mm were cut into 5 mm-wide strips using parallel blade cutter (the length setting was 10 mm).

Static water-contact-angle (θ_w) was measured on a contact anglemeter (Dataphysics Co., Germany) at ambient temperature using the sessile drop method and image analysis of the drop profile. The reported values were an average of 10 individual readings recorded within 5 s.

2.4. Scaffold seeding and culture

Circular discs, 10 mm in diameter, were punched out from n-chitin/PCL samples and disinfected by immersing in ethanol for 10 min, followed by three rinses with sterile phosphate-buffered

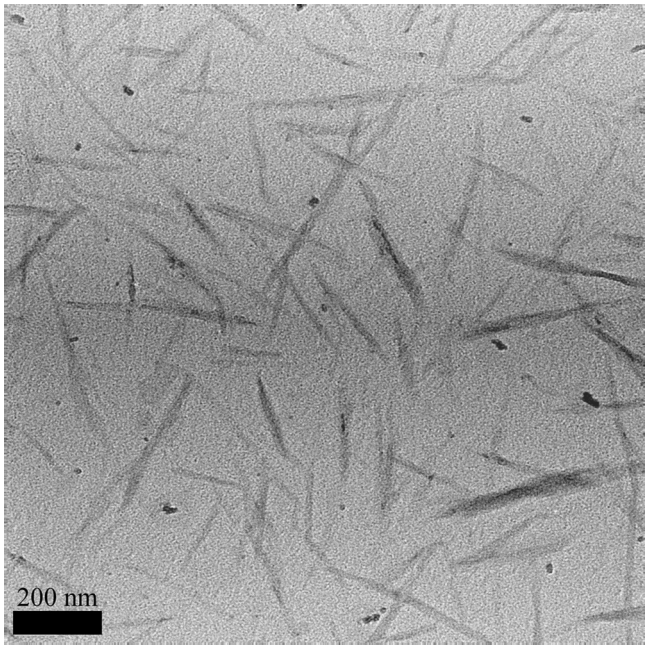

Fig. 1. Transmission electron micrograph of a dilute TFE suspension of chitin nanofibrils (scale bar = 200 nm).

solution (PBS) for 3 min, and then placed into a 48-well culture plate. Human dermal fibroblasts (hDF, Cascade Biologics C013-5 C) were seeded on each scaffold at a density of 100,000 cells per well and 400 μL culture medium (DMEM-F12 supplemented with 10% fetal bovine serum and 1% penicillin–streptomyocin) was added to each well. The scaffolds were then statically cultured under standard conditions (37 °C and 5% CO_2) in an incubator. One disk of each sample was removed after 1 and 14 days. Removed discs were fixed in 10% formalin for subsequent evaluation of cell morphology by SEM and fluorescent microscopy (Nikon TE300 microscope equipped with a DXM 1200 digital camera). For SEM imaging, the samples were dehydrated in a graded series of ethanol (50, 75 and 100%) and sputter-coated with gold. For fluorescent microscopy imaging, the sample was cryosectioned for slide mounting and stained by 4′-6-diamidino-2-phenylindole (DAPI) for 10 min.

3. Results and discussion

Fig. 1 shows the transmission electron micrograph of a dilute TFE suspension prepared by redispersing chitin nanofibril powders into TFE solvent. Within the visual field of microscope, individual chitin nanofibrils were uniformly distributed, and the estimated average length of chitin nanofibril was 300 nm and average width was 20 nm, thus, the aspect ratio L/d (L being the length and d the width or diameter) was around 15. This analysis demonstrates that chitin nanofibrils can redisperse well in the TFE solvent.

We found the mixtures of PCL and chitin nanofibril in TFE were rather clear, and it was easy to electrospin PCL and n-chitin/PCL solution or suspension in TFE on condition that the total solid content was controlled in the range of 8–10 wt%. The morphologies of electrospun fiber mats were studied by SEM. Fig. 2 shows the typical SEM images of electrospun neat PCL and n-chitin/PCL nanocomposite fiber mats. The corresponding fiber diameter measurements are given in Fig. 3. As shown in Fig. 2, all the fiber mats were homogeneous and beads within a single fiber were rarely visible. However, the addition of chitin nanofibrils induced a significant reduction in fiber diameter from over 1 μm (neat PCL) down to 200–400 nm (5–30% chitin nanofibril loading). Considering the actual concentrations of PCL in TFE, they varied depending on the loaded amount of chitin nanofibrils, starting at 150 mg cm^{-3} for neat PCL, 144 mg cm^{-3} for 5:95 n-chitin/PCL, reducing to 106 mg cm^{-3} for 30:70 n-chitin/PCL. Generally, the electrospinning solution with a low solid concentration tended to produce a fiber in smaller diameter. However, such a tremendous reduction in diameter in this case could not be only explained by the influence of the solid concentration. It was considered that the chitin nanofibril was positively

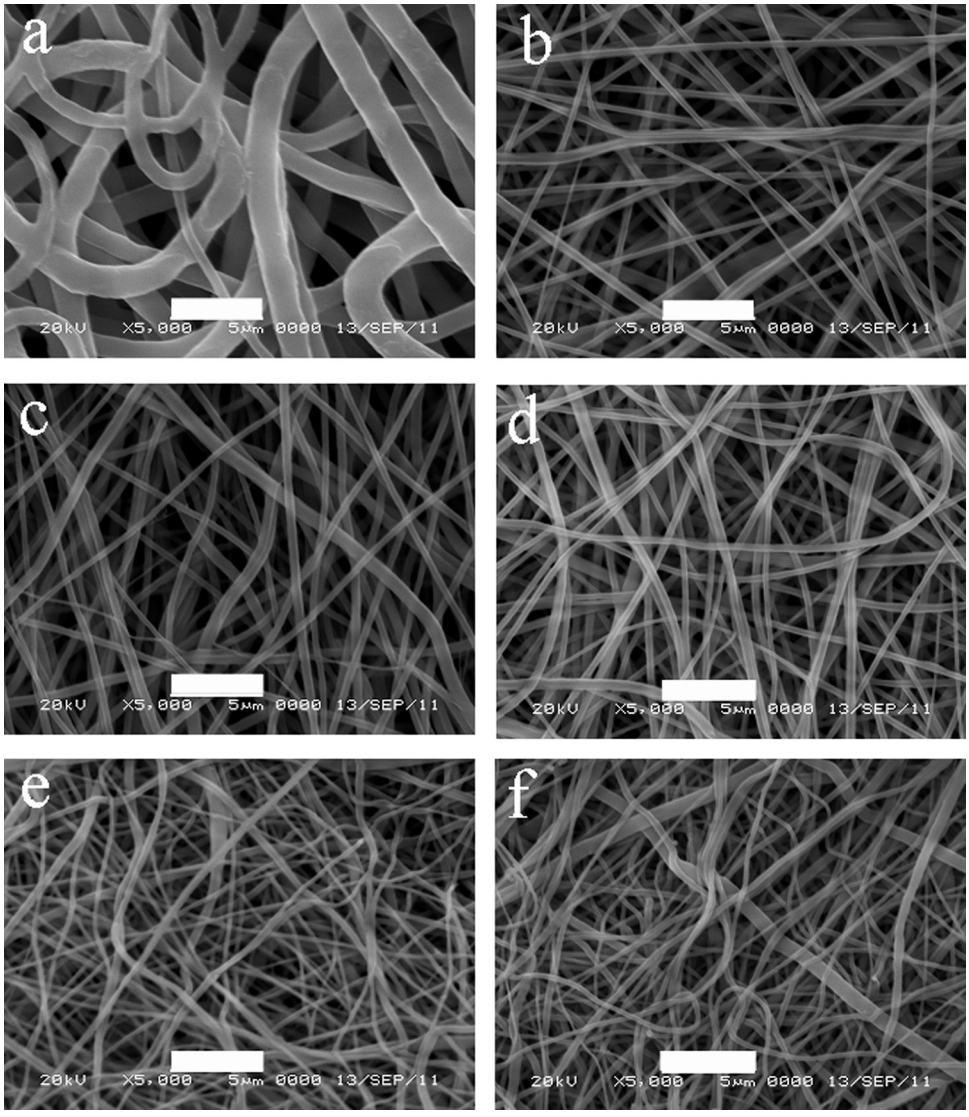

Fig. 2. Scanning electron micrographs of electrospun n-chitin/PCL fiber mats (a) 0:100; (b) 5:95; (c) 10:90; (d) 15:85; (e) 20:80 and (f) 30:70 (scale bar = 5 μm).

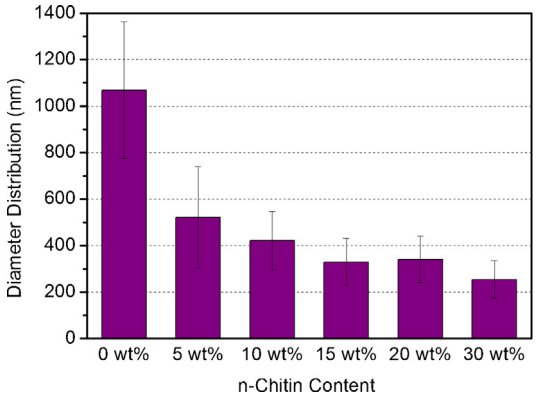

Fig. 3. Effect of chitin nanofibril content on the diameter distribution of n-chitin/PCL fibers (error bars show standard deviations based on randomly selected 80 fibers).

charged due to the presence of NH_4^+ cations on its surface, which were produced during the acid-treatment process. Thus, the addition of chitin nanofibrils was believed to enhance the electrostatic charge density of electrospinning solutions and induce more extensive filament stretching during jet whipping, ultimately resulting in a significant reduction in diameter of the electrospun nanofibers.

To confirm the inclusion of chitin nanofibrils in n-chitin/PCL fibers, all the fiber mats were subjected to analyze with FTIR spectroscopy. The spectra of PCL fiber mat, n-chitin/PCL (30:70) fiber mat and chitin nanofibril powders selected as samples are presented in Fig. 4(a). The typical peaks corresponding to PCL and chitin nanofibrils were both observed in the spectra of n-chitin/PCL fiber mats. The characteristic peak of ester group (1724 cm^{-1}) in all the n-chitin/PCL fiber mats were nearly the same, without any evident changes in comparison with the neat PCL fiber mat, implying the affinity between chitin nanofibril and PCL was relatively weak, that is, the hydrogen-bond interaction between chitin nanofibrils and PCL was not evident.

The WAXD patterns of the electrospun PCL and n-chitin/PCL fiber mats are shown in Fig. 4(b). Two typical crystalline diffraction peaks at $2\theta = \sim 21^\circ$ and $\sim 23^\circ$ for the as-spun PCL fiber mat were attributed to (1 1 0) and (2 0 0) crystal plane, respectively, however, an unknown peak at $2\theta = \sim 19^\circ$ appeared. For all composite fiber mats, a new diffraction peak at $2\theta = \sim 9^\circ$ attributed to the chitin nanofibril (0 2 0) crystal plane was observed and the diffraction peak at $2\theta = \sim 19^\circ$ gradually intensified with chitin nanofibril, which could be ascribed to the chitin nanofibril (1 1 0) crystal plane. However, the primary peak around $\sim 23^\circ$ attributed to the chitin nanofibril (1 3 0) crystal plane was not observed individually, due to the overlapping with that of PCL crystal plane. Apparent crystal size (L_{hkl}) of PCL could be estimated by Scherrer's equation: $L_{hkl} = K\lambda/\beta\cos\theta$, where λ was the X-ray wavelength of 1.54 Å, K was the shape factor, often assigned a value of 0.89, L_{hkl} was the average size of the crystals, θ was the Bragg angle, and β was the half-width of the diffraction at a scattering angle 2θ, assuming that the finite size of crystallites dominated the broadening of the X-ray reflections and neglecting instrumental broadening and possible imperfections of the crystal lattice (Sebe, Ham-Pichavant, Ibarboure, Koffi, & Tingaut, 2012). The apparent crystal sizes of PCL were obtained from the most prominent diffraction peak (1 1 0). The calculated L values showed that the crystal sizes of PCL in the nanocomposite fiber mats were slightly lower than that in the pure PCL fiber mat, suggesting that the introduction of chitin nanofibrils was deleterious for the packing of PCL molecular chains, and resulted in smaller crystals.

The effects of chitin nanofibrils on the thermal behavior of PCL matrix were investigated by DSC and TGA. The thermal parameters, including the melting temperature (T_m), enthalpy of fusion (ΔH_m), degree of crystallinity (X_c), and onset degradation temperature (T_{id}) for all fiber mats were summarized in Table 1. The incorporation of chitin nanofibrils slightly decreased the melting temperature T_m (from 61.0 to 58.7 °C), whereas increased the degree of crystallinity X_c, implying more but smaller PCL crystallites were formed within the electrospun nanocomposite fibers compared to the electrospun PCL fibers. This point was in good agreement with the above-mentioned result of WAXD. It was thought chitin nanofibrils could act as nucleating agents in the crystallization of PCL. Owing to the high specific area, PCL crystal growth was expected to be induced on the surface of chitin nanofibrils. However, during electrospinning, the very high shear stress and the very fast solvent evaporation caused rapid crystallization of PCL, which on the contrary restricted crystallite further growth. The TGA thermograms indicated the loading of chitin nanofibrils decreased the initial decomposition temperatures of fiber mats from 299 °C (0:100) to 245 °C (30:70), whereas the peak temperatures for the highest weight loss rate remained constant (around 397 °C) for all fiber mats. Thus, the decreased thermal stability was due to the presence of the chitin nanofibrils, which decomposed at lower temperature (T_{id} = 205 °C).

Table 1
Thermal properties of electrospun fiber mats derived from DSC and TGA thermograms.

Sample	T_m (°C)	ΔH_m (J g^{-1})	X_c[a]	T_{id} (°C)
0:100	61.0	71.4	0.45	299.1
5:95	61.4	71.2	0.48	295.2
10:90	61.4	68.6	0.49	288.5
15:85	61.4	68.5	0.51	269.1
20:80	59.4	62.4	0.50	273.9
30:70	58.7	54.6	0.50	244.9

[a] $X_c = \Delta H_m/\Delta H_m^\circ(1-w)$, with ΔH_m° = 157 J g^{-1} is the heat of fusion for 100% crystalline PCL (Habibi & Dufresne, 2008); w is the weight fraction of chitin nanofibril in the nanocomposite; the melting temperature T_m was taken as the peak temperature of the melting endotherm.

In order to determine the reinforcing effect of chitin nanofibrils on the mechanical properties of PCL electrospun fibers, DMA tests were conducted. Fig. 5(a) and (b) displays the plots of storage tensile modulus E' and loss angle tangent $\tan\delta$ as a function of temperature for all the fiber mats. At low temperature (below −55 °C), the storage modulus nearly kept constant with temperature, owing to the fact that the polymer was in the glassy state and molecular motions were largely restricted to vibration and short-range rotation. Around −55 °C, a mild, small drop in the storage modulus appeared for all the samples, i.e., in the glass–rubber transition zone, followed by a rubbery plateau region (−55 to 40 °C), i.e., an amorphous, rubbery, and crystalline domains coexisting region. This modulus drop was very small, in other words, the rubbery modulus was relatively large, which possibly resulted from the large degree of crystallinity of the matrix in that the crystalline regions can act as physical crosslinks so as to increase the modulus substantially. Moreover, the n-chitin/PCL nanocomposite fiber mats presented smaller modulus drops in comparison with neat PCL, because they had a higher degree of crystalinity as shown in the previous DSC results. It should be noted that the storage modulus of n-chitin/PCL nanocomposite fiber mats significantly increased by 1–2 orders of magnitude compared to neat PCL within the temperature range. This reinforcing effect mainly originated from the loading of chitin nanofibrils. At the melting temperature of PCL (around 50 °C), the second modulus drop related to the crystalline domains melting appeared. After this sharp modulus drop, an unexpected modulus plateau region occurred in some of n-chitin/PCL nanocomposite fiber mats. The plateau modulus remained constant from 50 to 80 °C, subsequently, a third modulus drop occurred due to unrecoverable deformations in the system. Since the matrix became viscous at this stage, this plateau region implied a stable

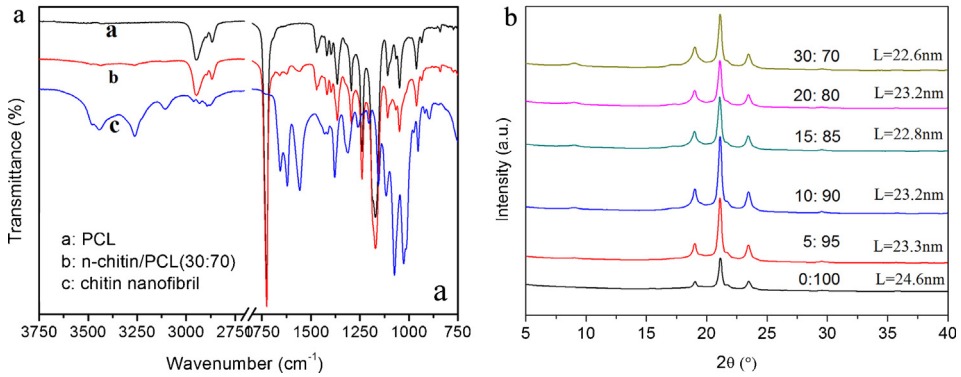

Fig. 4. (a) FTIR spectra of electrospun PCL, n-chitin/PCL fibrous mesh and chitin nanofibril powders and (b) WAXD patterns of electrospun PCL and n-chitin/PCL fiber mats.

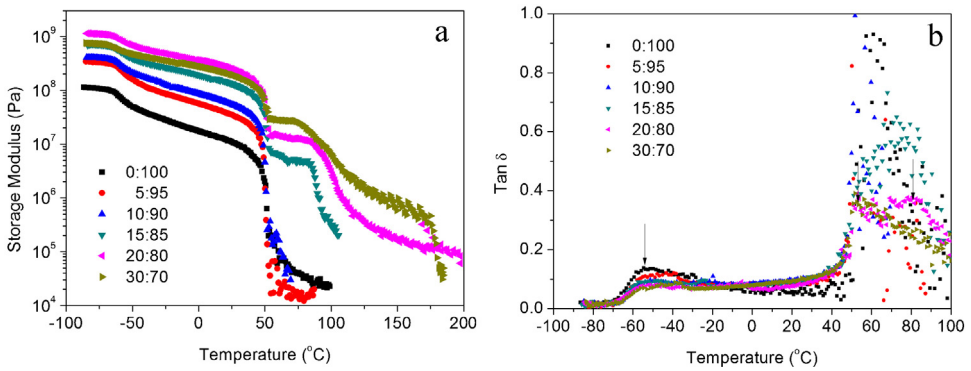

Fig. 5. (a) Storage tensile modulus E' and (b) loss angle tangent tan δ vs temperature at 1 Hz for the fiber mats.

rigid phase existed in the fused matrix, i.e., a rigid chitin nanofibril structure. Furthermore, the plateau modulus value increased with the chitin nanofibril loading, though if loading was less than 15 wt% the plateau region did not occur. It was considered that the chitin nanofibrils possibly located within the PCL matrix and arranged themselves along the fiber long axis, which had been proved in our previous study (Ji et al., 2012). When the PCL matrix melted, the rigid chitin nanofibrils could be as fiber's framework to keep modulus constant to a certain degree; however, the chitin nanofibrils lying in different fibers could not form a network structure due to 'disconnect' and also they could not rearrange themselves into a network within the viscous matrix, therefore, the modulus sharply dropped again at around 80 °C. Fig. 5(b) displays three peaks at ~−55 °C, ~50 °C and ~80 °C, which were directly linked to the three modulus drops, i.e., the glass–rubber transition zone, the rubber-viscosity flow transition zone, and the unrecoverable deformation zone, respectively.

Chitin is more hydrophilic than PCL, hence the addition of chitin nanofibrils into PCL will possibly change the wettability of the nanocomposites. Considering this point, the static water-contact-angle measurement was used to evaluate the surface wettability of the nanocomposites filled with different amount of chitin nanofibrils. As shown in Table 2, the contact angle of the nanocomposite fiber mat loaded with 5 wt% chitin nanofibrils unexpectedly increased in comparison with neat PCL, and the contact angle value continued to increase until chitin nanofibril loading up to 15 wt%, and then it started to decrease. When the chitin nanofibril content was up to 25 wt%, the contact angle substantially decreased to less than 90°, and ultimately attained fully wettability as the chitin nanofibril content increased up to 30 wt%. It was believed that the contact angle was not only dependent on the material composition but dependent on the surface morphology. Generally, the surface contact angles of fiber mats are usually larger than that of smooth surfaces in that the liquid–solid contact area decreases and the liquid-air contact area increases when a drop of water is placed on the surface of fiber mat (Cipitria et al., 2011). The finer fibers will produce a smaller liquid–solid contact area, leading to a higher contact angle. It can be said that the composition and the fiber diameter together determine the contact angles of fiber mats. In our case, the fiber diameters significantly decreased as long as chitin nanofibrils were incorporated. Initially, the chitin nanofibril content was low, and the fiber diameter became the dominant factor and leaded to the increase of contact angles. However, when more hydrophilic chitin nanofibrils were loaded, the composition factor exceeded the

Table 2
The measurement results of static water contact angle for n-chitin/PCL fiber mats.

Sample	0:100	5:95	10:90	15:85	20:80	25:75	30:70[a]
Contact angle (°)	117.8	123.4	126.1	125.8	122.0	83.9	–
Image						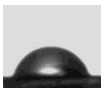	

[a] When a drop of water was placed on the sample, the drop disappeared immediately and left a water mark. This image was a snapshot.

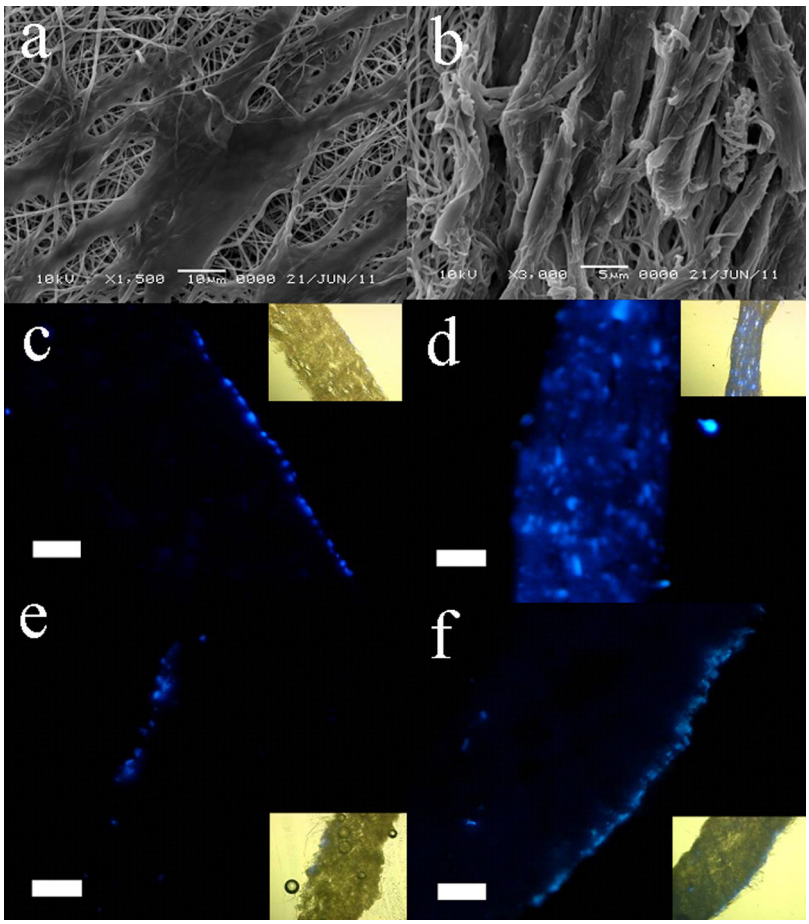

Fig. 6. Scanning electron microscopy micrographs of the surface (a) and cross-section (b) of n-chitin/PCL fiber mats (30:70) cultured over a period of 14 days; corresponding fluorescence microscopy images of the cross-section over a period of 1 day (c) and 14 days (d); fluorescence microscopy images of the cross-section of PCL fiber mats cultured over a period of 1 day (e) and 14 days (f). Insets are the images under nature light (scale bar is set to 100 μm).

surface morphology factor and dominated the surface wettability, ultimately producing a fully hydrophilic surface.

The effect of the incorporation of chitin nanofibril into PCL matrix on cell attachment and proliferation was preliminarily evaluated by seeding human dermal fibroblasts on the fiber mat scaffolds for periods of 1 and 14 days in vitro. Fig. 6(a) and (b) shows the surface and cross-section morphologies of the scaffold (30:70) cultured for 14 days. According to the micrographs, the cells not only spread on the surface of scaffold, but also penetrated and migrated inside the scaffold. It was difficult to differentiate individual cell in Fig. 6(b). It seemed that several cells grew together. For more convincing, fluorescent microscopy was used to verify whether they were cells in Fig. 6(b). Fig. 6(c) and (d) depicts the fluorescence microscopy images of the cross-section of scaffold (30:70) cultured for periods of 1 and 14 days. At day 1, cells just attached on the surface of scaffold, but at day 14, cells infiltrated into the scaffold, which was coincident with the SEM observation. As a contrast, the fluorescence microscopy images of the neat PCL scaffold cultured for periods of 1 and 14 days are presented in Fig. 6(e) and (f), respectively. Obviously, there was no evidence that cells infiltrated into the scaffold. Thus, the addition of chitin nanofibrils to PCL matrix could highly improve the cellular infiltration and migration as well, indicating a 3D cell growth. Commonly, the pores formed in the electrospun fibrous structure are smaller than the normal cell size of about 10–15 μm, which can inhibit cell infiltration. However, several studies (Li, Laurencin, Caterson, Tuan, & Frank, 2002; Shabani, Haddadi-Asl, Seyedjafari, Babaeijandaghi, & Soleimani, 2009; Zhang, Ouyang, Lim, Ramakrishna, & Huang, 2005) indicated that when cells performed amoeboid movement to migrate through the pores, they could push the surrounding fibers aside to expand the hole in that the small and loosely stacked fibers offer little resistance to cell movement. Thus, the cell was able to penetrate into the electrospun mat even though pores were smaller than the size of the cell. The main reason probably is that appropriate hydrophilicity and biochemical signals can promote cell-matrix interaction and hence facilitate cell ingrowth. In this regard, the current n-chitin/PCL nanocomposite fiber mat exhibited a surprising performance for cell infiltration. This could be explained by the change of surface wettability. In the contact angle tests mentioned previously it was proved that the surface hydrophilicity of scaffolds was highly improved if chitin nanofibril loading was more than 25 wt%, which facilitated fibroblasts attachment and infiltration. In addition, chitin based materials were reported to have biochemical activities such as polymorphonuclear cell activation, fibroblast activation, cytokine production, giant cell migration and simulation of type IV collagen synthesis (Jayakumar et al., 2011). The bioactivity of chitin might be another reason for promoting cell ingrowth, but it needs to be further investigated.

4. Conclusions

In this study, the nanocomposite fiber mats based on biodegradable polycaprolactone and chitin nanofibrils were successfully fabricated by means of electrospinning. The addition of chitin nanofibrils into PCL matrix produced some positive influence on

the mechanical and biological properties. For examples, the fiber diameter significantly decreased, the degree of crystallinity slightly increased, the storage modulus highly improved, the surface hydrophilicity increased, and the cell attachment and infiltration improved. In brief, it was confirmed the chitin nanofibril was a potential reinforcing and bioactive filler for PCL.

Acknowledgements

This work was supported by the program from the Natural Science Foundation of Shanghai (Grant No. 10ZR1400900), the National Natural Science Foundation of China (Grant No. 51303024) and the Fundamental Research Funds for the Central Universities.

References

Chen, J. P., & Chang, Y. S. (2011). Preparation and characterization of composite nanofibers of polycaprolactone and nanohydroxyapatite for osteogenic differentiation of mesenchymal stem cells. *Colloids and Surfaces B: Biointerfaces*, *86*, 169–175.

Cipitria, A., Skelton, A., Dargaville, T. R., Daltona, P. D., & Hutmacher, D. W. (2011). Design, fabrication and characterization of PCL electrospun scaffolds – A review. *Journal of Materials Chemistry*, *21*, 9419–9453.

Diba, M., Fathi, M. H., & Kharaziha, M. (2011). Novel forsterite/polycaprolactone nanocomposite scaffold for tissue engineering applications. *Materials Letters*, *65*, 1931–1934.

Dufresne, A. (2008). Polysaccharide nanocrystal reinforced nanocomposites. *Canadian Journal of Chemistry*, *86*, 484–494.

Erisken, C., Kalyon, D. M., & Wang, H. (2008). A hybrid twin screw extrusion/electrospinning method to process nanoparticle-incorporated electrospun nanofibres. *Nanotechnology*, *19*(165302), 8pp.

Fan, Y., Saito, T., & Isogai, A. (2008). Chitin nanocrystals prepared by TEMPO-mediated oxidation of α-chitin. *Biomacromolecules*, *9*, 192–198.

Habibi, Y., & Dufresne, A. (2008). Highly filled bionanocomposites from functionalized polysaccharide nanocrystals. *Biomacromolecules*, *9*, 1974–1980.

Ifuku, S., Nogi, M., Abe, K., Yoshioka, M., Morimoto, M., Saimoto, H., et al. (2009). Preparation of chitin nanofibers with a uniform width as alpha-chitin from crab shells. *Biomacromolecules*, *10*, 1584–1588.

Jayakumar, R., Chennazhi, K. P., Srinivasan, S., Nair, S. V., Furuike, T., & Tamura, H. (2011). Chitin scaffolds in tissue engineering. *International Journal of Molecular Science*, *12*, 1876–1887.

Ji, Y., Wolfe, P. S., Rodriguez, I. A., & Bowlin, G. L. (2012). Preparation of chitin nanofibril/polycaprolactone nanocomposite from a nonaqueous medium suspension. *Carbohydrate Polymers*, *87*, 2313–2319.

Jo, J. H., Lee, E. J., Shin, D. S., Kim, H. E., Kim, H. W., Koh, Y. H., et al. (2009). In vitro/in vivo biocompatibility and mechanical properties of bioactive glass nanofiber and poly(ε-caprolactone) composite materials. *Journal of Biomedical Materials Research Part B: Applied Biomaterials*, *91B*, 213–220.

Junkasem, J., Rujiravanit, R., Grady, B. P., & Supaphol, P. (2010). X-ray diffraction and dynamic mechanical analyses of α-chitin whisker-reinforced poly(vinyl alcohol) nanocomposite nanofibers. *Polymer International*, *59*, 85–91.

Kadokawa, J., Takegawa, A., Mine, S., & Prasad, K. (2011). Preparation of chitin nanowhiskers using an ionic liquid and their composite materials with poly(vinyl alcohol). *Carbohydrate Polymers*, *84*, 1408–1412.

Lee, S. J., Liu, J., Oh, S. H., Soker, S., Atala, A., & Yoo, J. J. (2008). Development of a composite vascular scaffolding system that withstands physiological vascular conditions. *Biomaterials*, *29*, 2891–2898.

Li, W. J., Laurencin, C. T., Caterson, E. J., Tuan, R. S., & Frank, K. K. (2002). Electrospun nanofibrous structure: A novel scaffold for tissue engineering. *Journal of Biomedical Materials Research*, *60*, 613–621.

Lu, Y., Weng, L., & Zhang, L. (2004). Morphology and properties of soy protein isolate thermoplastics reinforced with chitin whiskers. *Biomacromolecules*, *5*, 1046–1051.

McClure, M. J., Sell, S. A., Simpson, D. G., Walpoth, B. H., & Bowlin, G. L. (2010). A three-layered electrospun matrix to mimic native arterial architecture using polycaprolactone, elastin, and collagen: A preliminary study. *Acta Biomaterialia*, *6*, 2422–2433.

Muzzarelli, R. A. A. (2011a). Biomedical exploitation of chitin and chitosan via mechano-chemical disassembly, electrospinning, dissolution in imidazolium ionic liquids, and supercritical drying. *Marine Drugs*, *9*, 1510–1533.

Muzzarelli, R. A. A. (2011b). New techniques for optimization of surface area and porosity in nanochitins and nanochitosans. *Advances in Polymer Science*, *247*, 167–186.

Muzzarelli, R. A. A. (2011c). Nanochitins and nanochitosans, paving the way to ecofriendly and energy-saving exploitation of marine resources. In J. McGrath, & R. Hoefer (Eds.), *Comprehensive polymer science: Polymers for sustainable environment and energy*. Heidelberg: Springer.

Muzzarelli, R. A. A. (2011d). Chitin nanostructures in living organisms. In S. N. Gupta (Ed.), *Chitin formation and diagenesis*. New York: Springer.

Paillet, M., & Dufresne, A. (2001). Chitin whisker reinforced thermo-plastic nanocomposites. *Macromolecules*, *34*, 6527–6530.

Saeed, K., Park, S. Y., Lee, H. J., Baek, J. B., & Huh, W. S. (2006). Preparation of electrospun nanofibers of carbon nanotube/polycaprolactone nanocomposite. *Polymer*, *47*, 8019–8025.

Sebe, G., Ham-Pichavant, F., Ibarboure, E., Koffi, A. L. C., & Tingaut, P. (2012). Supramolecular structure characterization of cellulose II nanowhiskers produced by acid hydrolysis of cellulose I substrates. *Biomacromolecules*, *13*, 570–578.

Shabani, I., Haddadi-Asl, V., Seyedjafari, E., Babaeijandaghi, F., & Soleimani, M. (2009). Improved infiltration of stem cells on electrospun nanofibers. *Biochemistry and Biophysics Research Communications*, *382*(1), 129–133.

Sriupayo, J., Supaphol, P., Blackwell, J., & Rujiravanit, R. (2005). Preparation and characterization of α-chitin whisker-reinforced chitosan nanocomposite films with or without heat treatment. *Carbohydrate Polymers*, *62*, 130–136.

Wongpanit, P., Sanchavanakit, N., Pavasant, P., Bunaprasert, T., Tabata, Y., & Rujiravanit, R. (2007). Preparation and characterization of chitin whisker-reinforced silk fibroin nanocomposite sponges. *European Polymer Journal*, *43*, 4123–4135.

Woodruff, M. A., & Hutmacher, D. W. (2010). The return of a forgotten polymer-polycaprolactone in the 21st century. *Progress in Polymer Science*, *35*, 1217–1256.

Zhang, Y. Z., Ouyang, H., Lim, C. T., Ramakrishna, S., & Huang, Z. (2005). Electrospinning of gelatin fibers and gelatin/PCL composite fibrous scaffolds. *Journal of Biomedical Materials Research Part B: Applied Biomaterials*, *72B*(1), 156–165.

Zoppe, J. O., Peresin, M. S., Habibi, Y., Venditti, R. A., & Rojas, O. J. (2009). Reinforcing poly(ε-caprolactone) nanofibers with cellulose nanocrystals. *ACS Applied Materials & Interfaces*, *1*, 1996–2004.